HOKKAIDO UNIVERSITY

Intermittent PTH administration increases Bone-Specific Blood vessels and surrounding stromal cells in murine long bones

Shen Zhao[1,2,3], Tomoka Hasegawa[2#], Hiromi Hongo[2], Tomomaya Yamamoto[4], Miki Abe[2], Taiji Yoshida[2], Mai Haraguchi[2], Paulo Henrique Luiz de Freitas[5], Minqi Li[6], Kanchu Tei[3], and Norio Amizuka[2]

[1]Department of Endodontics, Ninth People's Hospital, Shanghai Jiaotong University, School of Medicine; Shanghai Key Laboratory of Stomatology & Shanghai Research Institute of Stomatology; National Clinical Research Center of Stomatology, Shanghai, China, [2]Developmental Biology of Hard Tissue, [3]Oral and Maxillofacial Surgery, Graduate School of Dental Medicine, Faculty of Dental Medicine, Hokkaido University, Sapporo, Japan, [4]Section of Dentistry, Camp Asaka, Japan Ground Self-Defense Forces, Tokyo, Japan, [5]Department of Dentistry, Federal University of Sergipe at Lagarto, Brazil, [6]Shandong Provincial Key Laboratory of Oral Biomedicine, The School of Stomatology, Shandong University, Jinan, China

Abbreviated Title: *Blood vessels in PTH-administered bone*

[#]Address for correspondence:

Tomoka Hasegawa, DDS, PhD

Developmental Biology of Hard Tissue

Graduate School of Dental Medicine, Hokkaido University

Kita 13 Nishi 7 Kita-ku

Sapporo, 060-8586, Japan

Tel/Fax: +81-11-706-4226

E-mail: hasegawa@den.hokudai.ac.jp

Abstract

To verify whether PTH acts on bone-specific blood vessels and on cells surrounding these blood vessels, 6-weeks-old male mice were subjected to vehicle (control group) or hPTH [1–34] (20 µg/kg/day, PTH group) injections for 2 weeks. Femoral metaphyses were used for histochemical and immunohistochemical studies. In control metaphyses, endomucin-positive blood vessels were abundant, but αSMA-reactive blood vessels were scarce. In the PTH-administered mice, the lumen of endomucin-positive blood vessels was markedly-enlarged. Moreover, many αSMA-positive cells were evident near the blood vessels, and seemed to derive from those vessels. These αSMA-positive cells neighboring the blood vessels showed features of mesenchymal stromal cells, such as immunopositivity for c-kit and tissue nonspecific alkaline phosphatase (TNALP). Thus, PTH administration increased the population of perivascular/stromal cells positive for αSMA and c-kit, which were likely committed to the osteoblastic lineage. To understand the cellular events that led to increased numbers and size of bone-specific blood vessels, we performed immunohistochemical studies for PTH/PTHrP receptor and VEGF. After PTH administration, PTH/PTHrP receptor, VEGF and its receptor flk-1 were consistently identified in both osteoblasts and blood vessels (endothelial cells and surrounding perivascular cells). Our findings suggest that exogenous PTH increases the number and size of bone-specific blood vessels while fostering perivascular/stromal cells positive for αSMA/TNALP/c-kit.

Introduction

Teriparatide, a recombinant form of the human parathyroid hormone (PTH), and more recently, abaloparatide, a recombinant analog to PTH-related peptide (PTHrP), are gradually becoming the preferred drugs for the treatment of osteoporosis [1-3]. The anabolic action of PTH and PTHrP has been demonstrated in clinical trials showing increased bone mass and reduced fracture rates in osteoporotic subjects receiving these drugs [3-5]. The earlier studies of our group showed that intermittent PTH administration promotes preosteoblastic proliferation and osteoblastic bone formation – with both processes being finely mediated by the cell coupling between osteoblasts and osteoclasts [6, 7]. Other studies have demonstrated the effect of PTH on blood vessels during bone healing. For instance, PTH-enhanced structural allograft healing has been linked to decreases in angiopoietin-2-mediated arteriogenesis [8]. Similarly, PTH1-34 treatment and/or increases in mesenchyme stem cells increased the number of vascular vessels, resulting in the stabilization of a femur fracture model in mice [9]. Therefore, PTH appears to not only affect bone cells but also blood vessels during bone healing. However, current studies have not determined whether PTH affects vascular endothelial cells in bone tissue without fracture healing or bone grafting, which may provide important insights into the osteo-vascular interactions associated with PTH treatment.

Recently, Kusumbe and Ramasamy's team characterized two subtypes of bone-specific endothelial cells, type H and type L [10]. While the type H cell is strongly positive for both CD31 and endomucin and is found near the metaphyseal growth plate, the type L cell has weak positivity for CD31 and endomucin and populates long bone's diaphyses [10, 11]. Interestingly, some degree of crosstalk between endomucin[high]-positive bone-specific blood vessels and osteoblastic cells seems to take place [10]: endomucin[high]-positive endothelial cells would secrete noggin, affecting both osteoblasts and chondrocytes, which in turn secrete vascular endothelial growth factor (VEGF) to sustain angiogenesis [10, 11]. Other studies have unveiled crosstalk involving endothelial cells, whereby vascular endothelial cells in arteries and arterioles expressed ephrinB2, whereas endothelial cells in veins expressed EphB4, a receptor for ephrinB2 [12]. Evidence on the interactions between EphB4 and ephrinB2 in the skeleton [13, 14] is growing, and since others have suggested that EphB4/ephrinB2 signalling acts as a coupling factor in bone cells [13, 14], it may be that EphB4-positive veins

and ephrinB2-reactive arteries can stimulate osteoblastic cells in one way or another. Taken together, these findings hint to an important and yet relatively neglected role for blood vessels in bone metabolism.

This putative role for the blood vessels in bone metabolism is supported by two related insights, the first being the gradual disappearance of perivascular cells in areas of accelerated bone modeling and remodeling. Considering a normal, homeostatic state, periosteal nutrient arteries and arterioles surrounded by vascular smooth muscle cells make their way toward a long bone's diaphyseal marrow [15]. These peripheral vascular smooth muscle cells gradually disappear to form sinusoidal capillaries that extend to the metaphyseal chondro-osseous junction; there, the peripheral vascular smooth muscle cell sheath is lost and discontinuous basement membranes are present [16]. Thus – and perivascular cells and vascular smooth muscle cells are normally not seen near vascular endothelial cells in the metaphyses – especially close to the growth plate, a site of endochondral ossification.

The second insight is the likely potential for trans-differentiation of vascular smooth muscle cells. Blood vessels are made of different cell types, roughly divided into inner, vascular endothelial cells and outer, perivascular cells [17]. A vascular smooth muscle cell is a type of perivascular cell that always covers arteries, veins, arterioles and venules and regulates vessel caliber [16]. α-Smooth muscle actin (αSMA) is a marker of vascular smooth muscle cells and myofibroblasts [18], but is also a hallmark of undifferentiated mesenchymal cells in calcified tissues [19]. It is plausible, therefore, that vascular smooth muscle cells may still have some potential for trans-differentiation [16, 18, 20]. Bone arteries are in fact reportedly covered with αSMA-positive cells that have the potential to differentiate into one of many mesenchymal lineages including osteoblasts [21–24].

Thus, the biological effects of PTH on bone-specific blood vessels and their constituent cells are yet to be fully explored. In this study, we have tried to determine whether intermittent PTH administration 1) affects the distribution and size of endomucin-positive, bone-specific blood vessels specific to bone, and 2) influences the population of stromal cells between osteoblasts and bone-specific blood vessels in mice.

Materials and methods

Animals

Six-week-old male C57BL/6J mice (n = 12, Japan CLEA, Tokyo, Japan) were handled according to Hokkaido University's guidelines for animal care and research use (approved study protocol #15-0032).   Mice were allocated to a control group receiving vehicle only (0.9% saline, n=12) or to a PTH group receiving hPTH [1-34] (Sigma-Aldrich Co., LLC., St. Louis, MO, n=12).   As previously described [6, 7], mice received 20 µg/kg/day of hPTH [1-34] every 12h for two weeks.

Specimen preparation

Before fixation, mice were anesthetized with an intraperitoneal injection of pentobarbital for body weight determination.   Afterward, all mice were perfused with 4% paraformaldehyde diluted in 0.1 M cacodylate buffer (pH 7.4) through the cardiac left ventricle 6 hours after receiving the last vehicle or hPTH [1-34] injection, as previously reported [7].   After perfusion with 4% paraformaldehyde, the femora and tibiae were extracted and immediately immersed in the same solution for 24 hours at 4 °C.   Then, specimens were washed in phosphate-buffered saline (PBS) for three days before decalcification with 10% or 4.13% EDTA-2Na for paraffin and epoxy resin embedding, respectively.   For paraffin embedding, samples were dehydrated in ascending ethanol solutions, soaked in xylene, and finally embedded in paraffin.   For epoxy resin embedding, samples were post-fixed with 1% osmium tetraoxide in 0.1 M cacodylate buffer for 8 hours at 4 °C, dehydrated in ascending acetone solutions, and finally embedded in epoxy resin (Epon 812).

Single immunohistochemical studies

Paraffin-embedded histological sections were used for an immunohistochemical panel of the following antigens: endomucin, αSMA, c-kit, PTH/PTH-related peptide (PTHrP) receptor, vascular endothelial growth factor (VEGF) and Flk-1.   Especially, the immunohistochemistry of PTH/PTHrP receptor, VEGF, and Flk-1 were performed on serial sections. After deparaffinization, standardized procedures for immunostaining were followed [25].   In brief, sections were treated for endogenous peroxidase inhibition with 0.3% H_2O_2 in PBS for 30 min,

and subsequently for nonspecific stain blocking with 1% bovine serum albumin (BSA; Serologicals Proteins Inc. Kankakee, IL) in PBS (1% BSA-PBS) for 20 min at room temperature. After that, sections were incubated with the corresponding pair of antibodies according to the antigen of interest (primary/secondary), as follows: 1) endomucin, rat antibody against endomucin (Santa Cruz Biotechnology, Inc., Dallas, TX, diluted 1:100) / horseradish peroxidase (HRP)-conjugated anti-rat IgG (Zymed Laboratories Inc., South San Francisco, CA, diluted 1: 100); 2) αSMA, mouse antibody against αSMA (Thermo Fisher Scientific Inc., Cheshire, UK, diluted 1: 400) / HRP-conjugated rabbit anti-mouse IgG (Bethyl Laboratories, Inc., Montgomery, TX); 3) c-kit, goat antibody against c-kit (R&D Systems Inc., Minneapolis, MN, diluted 1: 25) / HRP-conjugated anti-goat IgG (American Qualex Scientific Products, Inc., San Clemente, CA, diluted 1: 100); 4) PTH/PTHrP receptor, rabbit antibody against PTH/PTHrP receptor (Assay Biotechnology Company, Inc., Sunnyvale, CA, diluted 1: 50) / HRP-conjugated anti-rabbit IgG (Dako Denmark A/S, Produktionsvej, Denmark); 5) VEGF, rabbit antibody against VEGF (Santa Cruz Biotechnology, Inc., diluted 1: 100) / HRP-conjugated anti-rabbit IgG (Zymed, diluted 1:100); 6) Flk-1, mouse antibody against Flk-1 (Santa Cruz, diluted 1: 10) / HRP-conjugated rabbit anti-mouse IgG (Bethyl) **(See Supple Table 1)**

Reactions were assessed using 3, 3'-diaminobenzidine tetrahydrochloride (Dojindo Laboratories, Kumamoto, Japan). Then, specimens were observed under a Nikon Eclipse Ni microscope (Nikon Instruments Inc. Tokyo, Japan) and light microscopic images were acquired with a digital camera (Nikon DXM1200C, Nikon).

Double immunohistochemical studies

For endomucin/αSMA double immunohistochemical staining, dewaxed paraffin sections were incubated with 1% BSA-PBS, and then with mouse antibody against αSMA (Thermo Fisher), and subsequently with HRP-conjugated secondary antibody as described above. The immunostained sections were reacted with anti-endomucin antibody (Santa Cruz), followed by incubation with ALP-conjugated goat anti-rat IgG (Jackson Immuno Research Laboratories, Inc., West Grovw, PA). HRP visualization was described above, and ALP envision was performed by slide immersion in an aqueous solution containing 2.5 mg of naphthol AS-BI phosphate (Sigma) and 18 mg of Fast Blue RR salt (Sigma) diluted in 30 mL of a 0.1 M Tris-

HCl buffer (pH 8.5) for 15 min at 37 °C until immunoreactivity could be seen.

For immunofluorescent detection of endomucin/αSMA, sections were incubated with mouse antibody against αSMA, and then with FITC-conjugated goat anti-mouse IgG (MP Biomedicals. LLC., Solon, OH) diluted 1: 100 with 1% BSA-PBS. The sections were subsequently incubated with rat antibody against endomucin, and subsequently reacted with Alexa 594-conjugated rabbit anti-rat IgG (Thermo Fisher) diluted 1: 100. All sections were embedded by VECTASHIELD hard-set mounting medium with DAPI (Vector Laboratories, Inc. Burlingame, CA) and observed under light microscopy.

As with the immunofluorescent detection of endomucin/ephrinB2 and endomucin/EphB4, the sections immunostained for endomucin, which were followed with Alexa 594-labelling, were reacted with goat antibody against mouse ephrinB2 (R&D Systems) diluted 1: 50, or with goat antibody against mouse EphB4 (R&D Systems) diluted 1: 50 at 4°C overnight. After several washings in PBS, they were incubated with Alex 488-conjugated donkey anti-goat IgG (Abcam PLC., Cambridge, UK) for 1 hour.

For the detection of tissue nonspecific alkaline phosphatase (TNALP)/αSMA, dewaxed paraffin sections were incubated with mouse antibody against αSMA (Thermo Fisher), and then labelled with HRP-conjugated secondary antibody as described. The immuno-labeled sections were reacted with rabbit polyclonal antisera against TNALP diluted 1: 300 with 1% BSA–PBS [26]; then, they were incubated with ALP-conjugated goat anti-rabbit antibody (Jackson).

Transmission electron microscopy studies

Semi-thin sections of epoxy-resin embedding specimens were cut with an ultramicrotome (Sorvall MT-5000; Ivan Sorvall, Inc., Norwalk, CT), stained with toluidine blue staining and observed under a Nikon Eclipse E800 microscope (Nikon Instruments Inc. Tokyo, Japan). Ultra-thin sections obtained with an ultramicrotome were stained with uranyl acetate and lead citrate. These specimens were subjected to TEM observation (Hitachi H-7100, Hitachi Co., Tokyo, Japan) at 80 kV.

Quantification of the numbers of endomucin-positive, αSMA-positive, and EphB4-positive blood vessels, diameters and areas of blood vessels, and bone volume/tissue volume (BV/TV),

osteoblast surface/bone surface (Ob.s/BS), TNALP(+)areas/TV, and VEGF(+)cell areas/TV
ratios

A boxed area with 800 μm (width) x 1000 μm (length), the region of interest (ROI), located directly below the central bottom of the proximal femoral growth plate in the control and PTH-treated groups (n = 6 for each group) was used to quantify endomucin-positive, αSMA-positive, and EphB4-positive blood vessels, as well as blood vessel diameter and area indices, and bone volume/tissue volume (BV/TV), osteoblast surface/bone surface (Ob.s/BS), TNALP(+)areas/TV, and VEGF(+)areas/TV ratios.   Additionally, our study also determined the maximum diameter (length of the longest line joining two points within a blood vessel's outline and passing through its centroid), minimum diameter (length of the shortest line joining two points within the blood vessel's outline and passing through centroid), and mean diameter (average length of diameters measured at 2-degree intervals and passing through the blood vessel's centroid) of endomucin-immunopositive blood vessels.   Four images of different regions in the ROI at 200 x magnification were acquired to create a composite ROI image in order to obtain a sufficiently high-resolution image to determine the aforementioned indices with the Image-Pro Plus 6.2 software (Media Cybernetics, Inc., Bethesda MD).

RT-PCR and real time-PCR assessment

Total RNA was extracted from femora to evaluate *Gapdh, Endomucin, αSma, Ephb4, ephrinb2,* and *PTH/PTHrP receptor* gene expression.   The specimens were homogenized in 10 mL TRIzol reagent (Life Technologies Co. Carlsbad, CA) per 1 g of tissue to extract total RNAs.   The mixture was centrifuged at 15,000 rpm for 5 min at 4 °C to remove small debris.   The supernatant was then transferred to a new tube, which was vortexed for 15 s after the addition of 2 mL of chloroform.   The lysate was then transferred to a new tube and incubated for 5 min at RT.   After phase separation, the aqueous phase containing the RNA was transferred to a fresh new tube, after which the RNA was precipitated by adding 5 mL of isopropyl alcohol per 10 mL TRIzol reagent.   After 10 min of incubation at RT, the mixture was centrifuged for 60 min at 15,000 rpm at 4 °C.   The resulting RNA pellet was washed with 1 mL 75% ethanol and briefly air-dried.   The RNA was then dissolved in 30 μL DEPC-treated water.   First-strand cDNA was synthesized from 2 μg of total RNA with the SuperScript VlLO cDNA Synthesis Kit (Life Technologies).   The primer sequences used for RT-PCR are detailed in the

Supplementary Information **(Suppl. Table 2)**.   PCR was performed using a thermal cycler using the following thermal profile: denaturation at 94 °C for 30 s, annealing at 60 °C (for *Gapdh*) or 55 °C (for *Endomucin, αSma, Ephb4, ephrinb2, and PTH/PTHrP receptor*) for 30 s, extension at 72 °C for 30 s, and a final incubation at 72 °C for 10 min.   The RT-PCR products were electrophoresed on a 2% agarose gel containing ethidium bromide and visualized with the E-Gel Imager software (Life Technologies).   Real-time PCR assays were performed using Taqman probes (Applied Biosystems) to assess the expressions of the *Endomucin* (Mm00497495_m1),   *αSma*   (Mm00725412_s1),   *Ephb4*(Mm01201157_m1),   *Ephrinb2* (Mm00438670_m1), and *Pth1r* (Mm00441046_m1) genes. This step was conducted using a StepOne Real-Time PCR System (Applied Biosystems) and gene expression profiles were normalized to Gapdh (Mm99999915_g1) expression using the $2^{-\Delta\Delta Ct}$ method.

Statistical analysis

All statistical analyses were carried out using SPSS version 18.0.0 and analyzed for statistical significance by Student's t-test with significance set to *p<0.05*. Numerical data were presented as mean ± SD.

Results

Increased lumen diameters of bone-specific blood vessels and the appearance of αSMA-positive blood vessels after intermittent PTH administration

Despite the increased trabecular thickness and the consequent reduced intertrabecular space, endomucin-positive blood vessels appeared wider in diameter in the PTH group **(Fig. 1a, b)**. We then measured the maximum, minimum and mean diameters of endomucin-reactive blood vessels in the ROI of control and PTH-treated specimens **(Fig. 1e)**. The maximum diameter of endomucin-immunoreactive blood vessels were significantly larger in PTH-treated animals (224.53 ± 10.06 μm *vs. 339.22 \pm 14.58* μm, *p < 0.01*). Likewise, the mean diameter too was larger in the PTH group (121.37 ± 4.76 μm *vs. 144.01 \pm 4.63* μm, *p < 0.05*) **(Fig. 1e)**. The minimum vessel diameter was similar in specimens from the control and the PTH groups (73.16 ± 2.94 μm *vs. 73.26 \pm 2.32* μm, with no significance). In parallel with the increased lumen diameter, the area occupied by endomucin-reactive blood vessels was larger in the PTH-treated group (19841.02 ± 2585.61 μm^2 *vs. 28652.31 \pm 2413.11* μm^2, *p < 0.05*) **(Fig. 1f)**.

Interestingly, cell number and area of αSMA-immunopositive cells were markedly increased after PTH administration, while only few αSMA-positive blood vessels were seen in control specimens **(Figs. 1c, d)**.

Immunolocalization of endomucin-positive blood vessels and αSMA-immunoreactive cell after PTH administration.

In PTH-administered metaphyses, αSMA-positive cells extended from endomucin-reactive blood vessels and occupied the periphery of such vessels **(Figs. 2b, d)**. In control specimens, on the other hand, a small number of αSMA-positive cells surrounded few endomucin-positive blood vessels **(Figs. 2a, c)**. On higher magnification, some αSMA-positive cells lied close to endomucin-positive blood vessels, while other such cells were more distant from these vessels, showing a linear fibroblastic profile at the intertrabecular region **(Fig. 2e)**.

Distribution of ephrinB2-positive and EphB4-reactive cells after PTH administration

In the PTH group, endomucin-positive blood vessels seemed closer to ephrinB2-reactive osteoblasts **(Figs. 3a, b)**. After PTH treatment, most αSMA-positive fibroblastic cells

extending from the blood vessels reached the nearby ephrinB2-reactive osteoblastic layers.   In contrast, control specimens featured scarce αSMA-reactive cells around the blood vessels, without the pattern of cellular extension/migration toward the ephrinB2-positive osteoblastic layers **(Compare Figs. 3c and d)**.   Meanwhile, EphB4 immunoreactivity was detected on endomucin-positive blood vessels from both control and PTH groups, which suggests that these endomucin-positive blood vessels are veins and venules **(Figs. 4a-f)**.

The histochemical observations on the distribution of EphB4-positive, αSMA-positive, endomucin-positive blood vessels were verified in quantitative terms **(Fig. 4g)**.   The number of EphB4-positive, αSMA-positive, endomucin-positive blood vessels were 50.17 ± 18.45 vs 82.33 ± 14.63 (*p < 0.01*), 3.50 ± 2.17 vs 26.67 ± 7.58 (*p < 0.01*), 63.00 ± 18.01 vs 147 ± 42.37 (*p < 0.01*) in the ROIs of the control and the PTH group, respectively.   *Endomucin, αSma, ephrinb2,* and *Ephb4* expressions were found to be significantly upregulated after PTH administration according to RT-PCR and real-time PCR analyses (*endomucin*: 1.23 ± 0.07 in the control group and 1.78 ± 0.07 in the PTH group, *p< 0.001*; *αSma*: 0.65 ± 0.08 in the control group and 2.48 ± 0.37 in the PTH group, *p< 0.001*; *ephrinb2*: 0.90 ± 0.07 in the control group and 2.39 ± 0.56 in the PTH group, *p< 0.001*; *Ephb4*: 1.42 ± 0.09 in the control group and 1.80 ± 0.07 in the PTH group, *p< 0.001*) **(Fig. 4h-l)**.

Histochemical characteristics of αSMA-positive stromal cells extending from bone-specific blood vessels

We have examined the co-immunolocalization of TNALP and αSMA, as well as the ultrastructure of fibroblastic stromal cells located between the blood vessels and osteoblasts. In control specimens, αSMA-positive cells surrounded the blood vessels and did not show TNALP-reactivity **(Fig. 5a)**.   After PTH administration, however, the αSMA-positive cells that extended from the blood vessels were TNALP-positive **(Fig. 5b)**.   Still, TNALP-positive cells occupied a broader area than did αSMA-positive cells between blood vessels and osteoblasts.   In the control metaphyses, some bone marrow cells and few fibroblastic cells were positive for c-kit, a marker of mesenchymal stem cell [27] **(Fig. 5c)**.   After PTH administration, c-kit-reactive interstitial stromal cells occupied the same areas of the metaphyseal intertrabecular region as did αSMA-positive cells **(Fig. 5d)**.

We also compared the control and PTH-treated bone TNALP(+)areas/TV and Ob.S/BS

ratios in the ROI. Notably, both the TNALP(+)areas/TV and Ob.S/BS ratios were significantly elevated in the ROI where bone-specific blood vessels had significantly larger diameters and total luminal areas **(Please see Fig.1)**. The TNALP(+)areas/TV ratio was $1.75 \pm 0.15\%$ in the control group and $9.67 \pm 0.36\%$ in the PTH group (*p<0.001*) **(Fig. 5e)**, whereas Ob.S/Bs was $27.4 \pm 1.5\%$ in the control group and $56.9 \pm 2.1\%$ in the PTH group (*p<0.001*) **(Fig. 5f)**

Histologically, PTH-treated metaphyses showed blood vessels with walls thicker than those in control specimens **(Compare Fig. 6a-c)**. A variety of cell type was found among blood vessels and osteoblasts: some had long bodies with thin cytoplasmic processes and were distant from bone surfaces, while others had a transparent cell bodies different from mature osteoblasts **(Fig. 6c)**. Under TEM, it was possible to see that the elongated cytoplasmic processes of the interstitial cells made contact with osteoblastic cells. Moreover, there were blood vessels surrounded by vascular smooth muscle cells that made contact with osteoblasts **(Figs. 6d-g)**.

Immunolocalization of the PTH/PTHrP receptor, VEGF, and Flk-1 in PTH-treated metaphyses

As shown in **Fig. 7**, the control specimens mainly exhibited PTH/PTHrP receptors in the osteoblasts **(Fig. 7a)**, whereas the PTH-treated specimens exhibited PTH/PTHrP receptor immunopositivity not only in the osteoblasts but also in blood vessels and neighboring cells **(Fig. 7b)**. Consistent with these results, PTH treatment significantly increased PTH/PTHrP receptor mRNA in the PTH group (the gene expression ratios were 0.80 ± 0.05 in the control group and 2.07 ± 0.27 in PTH group, *p<0.001*) **(Fig. 7g, h)**. The control metaphyses hardly exhibited either VEGF or Flk-1 immunoreactivity **(Fig. 7c, e)**. After PTH administration, however, VEGF and Flk-1 immunopositivity was detectable mainly in osteoblasts and blood vessels/nearby cells **(Fig. 7d, f)**. Additionally, PTH-treated metaphyses had significantly higher VEGF(+)areas/TV ratios than the controls **(Fig. 7i)**.

Discussion

In this study, we have demonstrated that intermittent PTH administration affects bone-specific blood vessels and cells neighboring the blood vessels. We have reported elsewhere that intermittent PTH administration fostered osteoblastic bone formation and proliferation of Runx2-positive/TNALP-reactive preosteoblasts [6, 7]. Our current observations suggest that αSMA-positive cells surrounding the blood vessels are affected by exogenous PTH – presumably increasing the number of such cell type. This suggestion is strengthened by our finding of intense PTH/PTHrP receptor immunoreactivity in blood vessels following PTH administration, which ratified our earlier report on the expression of PTH/PTHrP receptor by vascular endothelial cells in the kidney [28]. Additional support to our conjecture comes from the study by Jiang et al., who showed that PTH treatment promotes vascularized bone regeneration by improving blood vessel formation and increasing the osteogenic potential of aged bone marrow mesenchymal stem cells [29]. Taken together, these evidences suggest a biological effect of PTH on blood vessels.

An exciting finding of this study is the increase in the number and in the diameter of blood vessels after PTH treatment, along with the growth in the population αSMA-positive/ c-kit-reactive cells –which not only surrounded the blood vessels, but extended from the vicinity of these blood vessels toward the osteoblastic cell layer. Even though the intertrabecular space became narrower as consequence of PTH-driven increased bone formation, the diameter of bone-specific blood vessels was enlarged **(Fig. 1)**. It is known that teriparatide causes a temporary drop in blood pressure, which is likely due to decreased arterial pressure. Studies with rats, dogs and rabbits showed that their aortas relaxed after PTH administration, thus inducing temporary blood hypotension [30]. Similarly, PTH reportedly induced the relaxation of cultured rat aorta vascular smooth muscle cells by increasing intracellular cyclic AMP [31, 32]. In contrast to this PTH-driven relaxation of vascular smooth muscle cells, most metaphyseal blood vessels in our study formed EphB4-reactive venous sinusoids lacking tunica media coverage and continuous basement membranes. Therefore, the enlarged blood vessels seen in PTH-treated bones did not seem to be directly involved with PTH-driven arterial relaxation.

The movement of αSMA-positive stromal cells away from the blood vessels may "pull" vascular endothelial cells with them, thus widening the lumen of the blood vessels. Moreover, we have registered the increased number of endomucin-immunoreactive/EphB4-positive blood vessels in the metaphysis. Dhillon *et al.* demonstrated that intermittent treatment with recombinant PTH enhanced structural allograft healing via two processes: (1) anabolic effects on new bone formation by inducing small vessel angiogenesis, and (2) inhibition of large vessels by arteriogenesis [8]. Intermittent PTH administration reportedly stimulates angiopoietin-1 gene expression but reduces the expression of the angiopoietin-2 gene, indicating that downregulation of angiopoietin-2-mediated arteriogenesis is a critical therapeutic mechanism of PTH for bone repair. In our study, the increases in blood vessels in PTH-treated metaphyses appeared to be consistent with Dhillon's observation. The numbers of αSMA-positive blood vessels were increased after PTH administration; however, many αSMA-positive cells migrated from the blood vessels instead of forming mature blood vessels with the tunica media of αSMA-positive vascular smooth muscles (*i.e.,* arteriogenesis). Our study did not employ a bone repair model; however, our mouse model results largely support those of Dhillon et al.

It is also interesting that αSMA-positive cells formed thick tunica media in metaphyseal blood vessels while spreading among osteoblasts and blood vessels in the intertrabecular spaces. The αSMA-positive stromal cells extending from the blood vessels toward the osteoblastic layer seem to be undifferentiated mesenchymal cells that also expressed c-kit and TNALP. A recent report suggested that c-kit was expressed by fetal, but not by postnatal skeletal progenitors [34]. Consistently, we hardly detected c-kit-reactive stromal cells in control specimens **(Fig. 5)**. Jiang *et al.* reported that PTH directly facilitated the proliferation of vascular endothelial cells and indirectly enhanced angiogenesis by promoting mesenchymal stem cell angiogenic differentiation [9]. Based on our observations, the cells positive for αSMA/TNALP/c-kit that extend from the PTH-treated blood vessels may include mesenchymal stem cells, which could then differentiate into vascular endothelial cells. In contrast, another study demonstrated the occurrence of transcortical perivascular cells near blood vessels in cortical bone and their osteogenic potential contributed to new osteoblast formation [24]. Therefore, the cells positive for αSMA/TNALP/c-kit derived from the PTH-treated blood vessels may differentiate into both vascular endothelial cells and osteoprogenitor cells.

14

However, given that both osteoblastic cells and vascular endothelial cells possess the PTH/PTHrP receptor, it seems necessary to determine whether PTH acts predominantly from bone to blood vessels or vice versa to recruit the cells positive for αSMA/TNALP/c-kit between the blood vessels and osteoblasts.

The intimate connection between blood vessels and bone tissues has been subjected to scientific scrutiny [38]. Since the bone matrix is highly vascularized, the assumption was that blood vessels were delivery channels for oxygen, nutrients, growth factors, and hormones, all the while taking part in hematopoiesis at the neighboring bone marrow [17]. That may not be the case: recently, it has been demonstrated that there is a network of transcortical capillaries that acts as a mainstay for blood circulation in long bones [39]. In addition, Kusumbe, Ramasamy et al. reported on a bone-specific, CD31^{high}/endomucin^{high} subtype of blood vessels and proposed that angiogenesis also plays an important role in bone development and remodeling [10, 11].

The putative site for osteo-vascular interaction may be the region filled with the αSMA-positive/c-kit-reactive interstitial stromal cells between the blood vessels and the bone surfaces. In fact, many cell types were identified in that area under higher magnification **(Fig. 6)**. Some of these cells extended long cytoplasmic processes linearly and parallel to the bone surfaces. Judging from the cell shape and the long cytoplasmic processes, this cell may well be the telocyte discovered in 2003 [40]. Telocytes are fibroblast-like cells with extremely long but thin cellular processes. However, telocytes have not been described in bone so far and, therefore, further examination is mandatory.

Considering our present findings and the supporting literature, we postulate that PTH, apart from affecting the number and the size of bone-specific blood vessels, also promotes the proliferation of αSMA-positive cells surrounding the blood vessels. Once proliferated, these αSMA-positive/c-kit-reactive interstitial stromal cells may differentiate into vascular smooth muscle cells or into a less differentiated cell type that is possibly committed to the osteogenic lineage. The wide distribution of PTH/PTHrP receptor expression and the variety of cell-type among the blood vessels and bone surfaces - at least in part - makes this postulation plausible.

Ethical standards

All animal experiments in this study were conducted under the Hokkaido University Guidelines for Animal Experimentation (approved research proposal #15-0032).

Competing interests

The authors declare no competing interests.

Contributors

Hasegawa T designed the study and prepared the first draft of the paper as a corresponding author. Zhao S is the researcher mainly in charge of this work, including RT-PCR, immunohistochemistry and TEM observation experiments. Hongo H, Abe M, Yoshida T contributed to the experimental work including the preparation of paraffin samples of PTH-administered mice. Yamamoto T was responsible for statistics. Freitas PHL, Li M, Tei K and Amizuka N participated in the discussion, editing and formatting of the manuscript. All authors revised the paper for intellectual content and approved its final version.

References

1. Schweser KM, Crist BD (2017) Osteoporosis: a discussion on the past 5 years. Curr Rev Musculoskelet Med 10: 265–274.

2. Orwoll E, Scheele W, Paul S, Adami S, Syversen U, Diez-Perez A, Kaufman JM, Clancy AD, Gaich GA (2003) The effect of teriparatide [human parathyroid hormone (1–34)] therapy on bone density in men with osteoporosis. J Bone Miner Res 18: 9–17.

3. Cosman F, Hattersley G, Hu MY, Williams GC, Fitzpatrick LA, Black DM (2017) Effects of Abaloparatide-SC on Fractures and Bone Mineral Density in Subgroups of Postmenopausal Women With Osteoporosis and Varying Baseline Risk Factors.   J Bone Miner Res 32(1):17–23.

4. Skripitz R, Aspenberg P (2004) Parathyroid hormone--a drug for orthopedic surgery? Acta Orthop Scand 75: 654–662.

5. Moreira CA, Fitzpatrick LA, Wang Y, Recker RR.: Effects of abaloparatide-SC (BA058) on bone histology and histomorphometry (2017) The ACTIVE phase 3 trial. Bone 97: 314–319.

6. Luiz de Freitas PH, Li M, Ninomiya T, Nakamura M, Ubaidus S, Oda K, Udagawa N, Maeda T, Takagi R, Amizuka N (2009) Intermittent PTH administration stimulates pre-osteoblastic proliferation without leading to enhanced bone formation in osteoclast-less c-fos(-/-) mice. J Bone Miner Res 24: 1586–1597.

7. Yamamoto T, Hasegawa T, Sasaki M, Hongo H, Tsuboi K, Shimizu T, Ohta M, Haraguchi M, Takahata T, Oda K, Freitas PHL, Takakura A, Takao-Kawabata R, Isogai Y, Amizuka N (2016) Frequency of teriparatide administration affects the histological pattern of bone formation in young adult male mice. Endocrinology 157: 2604–2620.

8. Dhillon RS, Xie C, Tyler W, Calvi LM, Awad HA, Zuscik MJ, O'Keefe RJ, Schwarz EM (2013) PTH-enhanced structural allograft healing is associated with decreased

angiopoietin-2-mediated arteriogenesis, mast cell accumulation, and fibrosis. J Bone Miner Res. 28(3):586-597.

9. Jiang X, Xu C, Shi H, Cheng Q (2019) PTH 1-34 improves bone healing by promoting angiogenesis and facilitating MSCs migration and differentiation in a stabilized fracture mouse model. PloS One 14(12): e0226163.

10. Kusumbe AP, Ramasamy SK, Adams RH (2014) Coupling of angiogenesis and osteogenesis by a specific vessel subtype in bone. Nature 507: 323–328.

11. Ramasamy SK, Kusumbe AP, Wang L, Adams RH (2014) Endothelial Notch activity promotes angiogenesis and osteogenesis in bone. Nature 507: 376–380.

12. Wang HU, Chen ZF, Anderson DJ (1998) Molecular distinction and angiogenic interaction between embryonic arteries and veins revealed by ephrin-B2 and its receptor Eph-B4. Cell 93(5): 741–753.

13. Rundle CH, Xing W, Lau KW, Mohan S (2016) Bidirectional ephrin signaling in bone. Osteoporosis Sarcopenia 2: 65–76.

14. Zhao C, Irie N, Takada Y, Shimoda K, Miyamoto T, Nishiwaki T, Suda T, Matsuo K (2006) Bidirectional ephrinB2-EphB4 signaling controls bone homeostasis. Cell Metab 4: 111–121.

15. Ramasamy SK (2017) Structure and functions of blood vessels and vascular niches in bone. Stem Cells Int 2017: 5046953.

16. Armulik A, Genove G, Betsholtz C (2011) Pericytes: developmental, physiological, and pathological perspectives, problems, and promises. Dev Cell 21: 193–215.

17. Sivaraj KK, Adams RH (2016) Blood vessel formation and function in bone. Development 143: 2706–2715.

18. Aizman I, Holland WS, Yang C, Bates D (2016) alphaSMA Expression in Large Colonies of Colony-Forming Units-Fibroblast as an Early Predictor of Bone Marrow MSC Expandability. Cell Med 8: 79–85.

19. Hosoya A, Nakamura H, Ninomiya T, Yoshiba K, Yoshiba N, Nakaya H, Wakitani S, Yamada H, Kasahara E, Ozawa H (2006) Immunohistochemical Localization of alpha-Smooth Muscle Actin During Rat Molar Tooth Development. J Histochem Cytochem 54(12): 1371–1378.

20. Matthews BG, Grcevic D, Wang L, Hagiwara Y, Roguljic H, Joshi P, Shin DG, Adams DJ, Kalajzic I (2014) Analysis of alphaSMA-labeled progenitor cell commitment identifies notch signaling as an important pathway in fracture healing. J Bone Miner Res 29: 1283–1294.

21. Kusumbe AP, Ramasamy SK, Itkin T, Mae MA, Langen UH, Betsholtz C, Lapidot T, Adams RH (2016) Age-dependent modulation of vascular niches for haematopoietic stem cells. Nature 532: 380–384.

22. Kunisaki Y, Bruns I, Scheiermann C, Ahmed J, Pinho S, Zhang D, Mizoguchi T, Wei Q, Lucas D, Ito K, Mar JC, Bergman A, Frenette PS (2013) Arteriolar niches maintain haematopoietic stem cell quiescence. Nature 502: 637–643.

23. Mendez-Ferrer S, Michurina TV, Ferraro F, Mazloom AR, Macarthur BD, Lira SA, Scadden DT, Ma'ayan A, Enikolopov GN, Frenette PS (2010) Mesenchymal and haematopoietic stem cells form a unique bone marrow niche. Nature 466: 829–834.

24. Root SH, Wee N K-Y, Novak S, Rosen CJ, Baron R, Matthews BG, Kalajzic I (2020) Perivascular osteoprogenitors are associated wih transcortical channels of long bones. Stem Cell 38: 769-781.

25. Hasegawa T, Yamamoto T, Sakai S, Miyamoto Y, Hongo H, Qiu Z, Abe M, Takeda S, Oda K, de Freitas PHL, Li M, Endo K, Amizuka N (2019) Histological Effects of the Combined Administration of Eldecalcitol and a Parathyroid Hormone in the Metaphyseal Trabeculae

of Ovariectomized Rats. J Histochem Cytochem. 67(3): 169–184.

26. Oda K, Amaya Y, Fukushi-Irié M, Kinameri Y, Ohsuye K, Kubota I, Fujimura S, Kobayashi J (1999) A general method for rapid purification of soluble versions of glycosylphosphatidylinositol-anchored proteins expressed in insect cells: an application for human tissue-nonspecific alkaline phosphatase. J Biochem 126:694-699.

27. Weiwen Deng (2010) Mesenchymal Stem Cells Express C-Kit. Circ Res. 107(10):e17.

28. Amizuka N, Lee HS, Kwan MY, Arazani A, Warshawsky H, Hendy GN, Ozawa H, White JH, Goltzman D (1997) Cell-specific expression of the parathyroid hormone (PTH)/PTH-related peptide receptor gene in kidney from kidney-specific and ubiquitous promoters. Endocrinology 138(1): 469–481.

29. Jiang L, Zhang W, Wei L, Zhou Q, Yang G, Qian N, Tang Y, Gao Y, Jiang X (2018) Early effects of parathyroid hormone on vascularized bone regeneration and implant osseointegration in aged rats. Biomaterials 179: 15–28.

30. Pang PK, Tenner Jr TE, Yee JA, Yang M, Janssen HF (1980) Hypotensive action of parathyroid hormone preparations on rats and dogs. Proc Natl Acad Sci. USA. 77 (1): 675–678.

31. Nickols GA (1985) Increased cyclic AMP in cultured vascular smooth muscle cells and relaxation of aortic strips by parathyroid hormone. Eur J Pharmacol. 116(1-2):137-144.

32. Nickols GA, Metz MA, Cline WH Jr (1986) Endothelium-independent linkage of parathyroid hormone receptors of rat vascular tissue with increased adenosine 3',5'-monophosphate and relaxation of vascular smooth muscle. Endocrinology 119(1):349-356.

33. Ding L, Saunders TL, Enikolopov G, Morrison SJ (2012) Endothelial and perivascular cells maintain haematopoietic stem cells. Nature, 481: 457–462.

34. Di Demi He, Xinyu Thomas Tang, Wenjie Dong, Guizhong Cui, Guangdun Peng, Xiujuan

Yin, Yujie Chen, Naihe Jing, Bo O Zhou (2020) C-kit expression distinguishes fetal from postnatal skeletal progenitors.   Stem Cell Reports 14(4): 614–630.

35. Rey A, Manen D, Rizzoli R, Ferrari SL, Caverzasio J (2007) Evidences for a role of p38 MAP kinase in the stimulation of alkaline phosphatase and matrix mineralization induced by parathyroid hormone in osteoblastic cells. Bone 41: 59–67.

36. Nakajima A, Shimoji N, Shiomi K, Shimizu S, Moriya H, Einhorn TA, Yamazaki M (2002) Mechanisms for the enhancement of fracture healing in rats treated with intermittent low-dose human parathyroid hormone (1-34). J Bone Miner Res 17: 2038–2047.

37. Hirota S, Takaoka K, Hashimoto J, Nakase T, Takemura T, Morii E, Fukuyama A, Morihana K, Kitamura Y, Nomura S (1994) Expression of mRNA of murine bone-related proteins in ectopic bone induced by murine bone morphogenetic protein-4. Cell and tissue research 277: 27–32.

38. Portal-Nunez S, Lozano D, Esbrit P (2012) Role of angiogenesis on bone formation. Histol Histopathol 27: 559–566.

39. Grüneboom A, Hawwari I, Weidner D, Culemann S, Müller S, Henneberg S, Henneberg S, Brenzel A, Merz S, Bornemann L, Zec K, Wuelling M, Kling L, Hasenberg M, Voortmann S, Lang S, Baum W, Ohs A, Kraff O, Quick HH, Jäger M, Landgraeber S, Dudda M, Danuser R, Stein JV, Rohde M, Gelse K, Garbe AI, Adamczyk A, Westendorf AM, Hoffmann D, Christiansen S, Engel DR, Vortkamp A, Krönke G, Herrmann M, Kamradt T, Schett G, Hasenberg A, Gunzer M (2019) A network of trans-cortical capillaries as mainstay for blood circulation in long bones. Nature Metabolism 1:236–250.

40. Marini M, Rosa I, Ibba-Manneschi L, Manetti M (2018) Telocytes in skeletal, cardiac and smooth muscle interstitium: morphological and functional aspects. Histol Histopathol 33: 1151–1165.
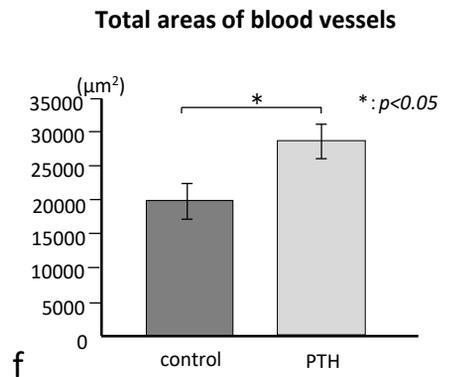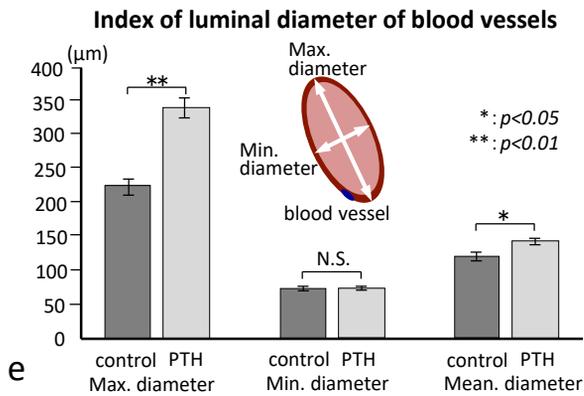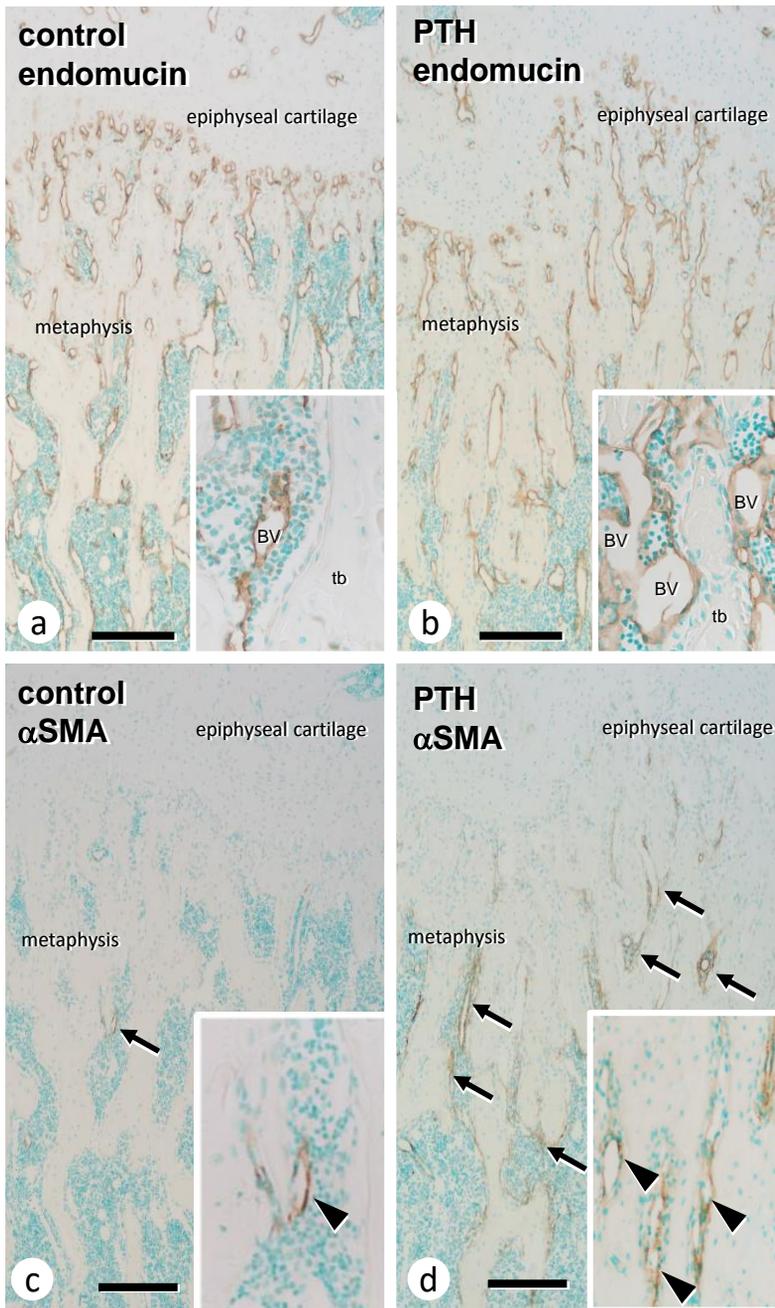
control
endomucin

epiphyseal cartilage

metaphysis

BV

tb

a

PTH
endomucin

epiphyseal cartilage

metaphysis

BV

BV

BV

tb

b

control
αSMA

epiphyseal cartilage

metaphysis

c

PTH
αSMA

epiphyseal cartilage

metaphysis

d

Index of luminal diameter of blood vessels

(μm)

400
350
300
250
200
150
100
50
0

Max.
diameter

Min.
diameter

blood vessel

* : *p<0.05*
** : *p<0.01*

**

N.S.

*

control   PTH
Max. diameter

control   PTH
Min. diameter

control   PTH
Mean. diameter

e

Total areas of blood vessels

(μm^2)

35000
30000
25000
20000
15000
10000
5000
0

* : *p<0.05*

*

control   PTH

f

Figure 1

Figure 2

Figure 3

endomucin Control

BV
tb
BV

a

EphB4

BV
tb
BV

b

Merged (endomucin/EphB4)

BV
tb
BV

c

PTH

tb
BV
tb
BV

d

tb
BV
tb
BV

e

tb
BV
tb
BV

f

(N)

*: *p<0.01*

Numbers of immunopositive cells

control PTH
EphB4(+)

control PTH
αSMA(+)

control PTH
endomucin(+)

g

Gapdh *endomucin* *α-sma* *ephrin b2* *Ephb4*

control PTH control PTH control PTH control PTH control PTH

h

endomucin

Relative Expression Ratio

p<0.001

control   PTH

i

a-sma

Relative Expression Ratio

p<0.001

control   PTH

j

ephrinb2

Relative Expression Ratio

p<0.001

control   PTH

k

Ephb4

Relative Expression Ratio

p<0.001

control   PTH

l

Figure 4

Figure 5

Figure 6

Control metaphysis
PTH/PTHrP receptor

BV

ob

tb

a

PTH metaphysis
PTH/PTHrP receptor

BV

tb

ob

b

BV

ob

tb

**Control
VEGF**

BV

ob

tb

c

**PTH
VEGF**

BV

ob

tb

ob

d

**Control
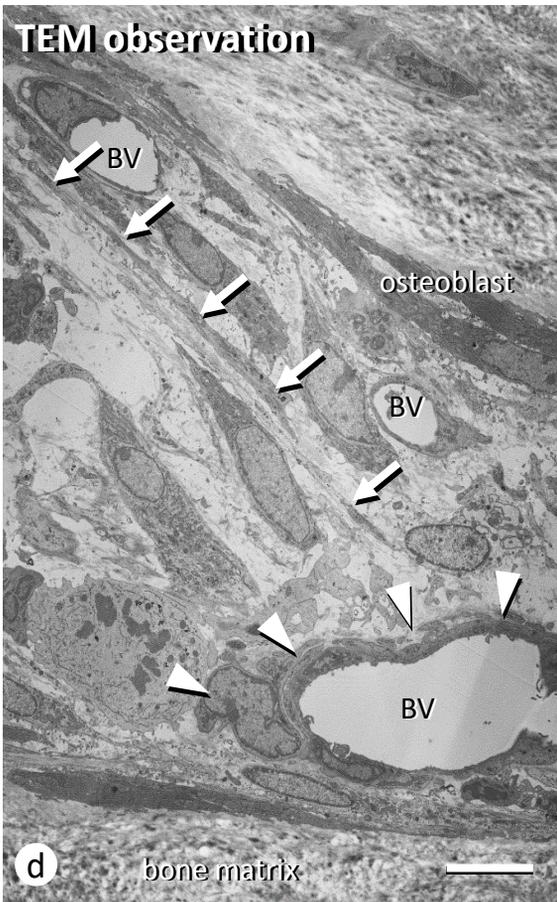Flk-1**

BV

ob

tb

e

**PTH
Flk-1**

ob

BV

tb

f

PTH/PTHrP receptor

control   PTH

g

Index of PTH/PTHrP receptor

p<0.001

Relative Expression Ratio

2.5

2.0

1.5

1.0

0.5

0

control   PTH

h

VEGF(+)areas/TV

(%)

p<0.001

Percentage of VEGF(+)areas/TV

8

6

4

2

0

control   PTH
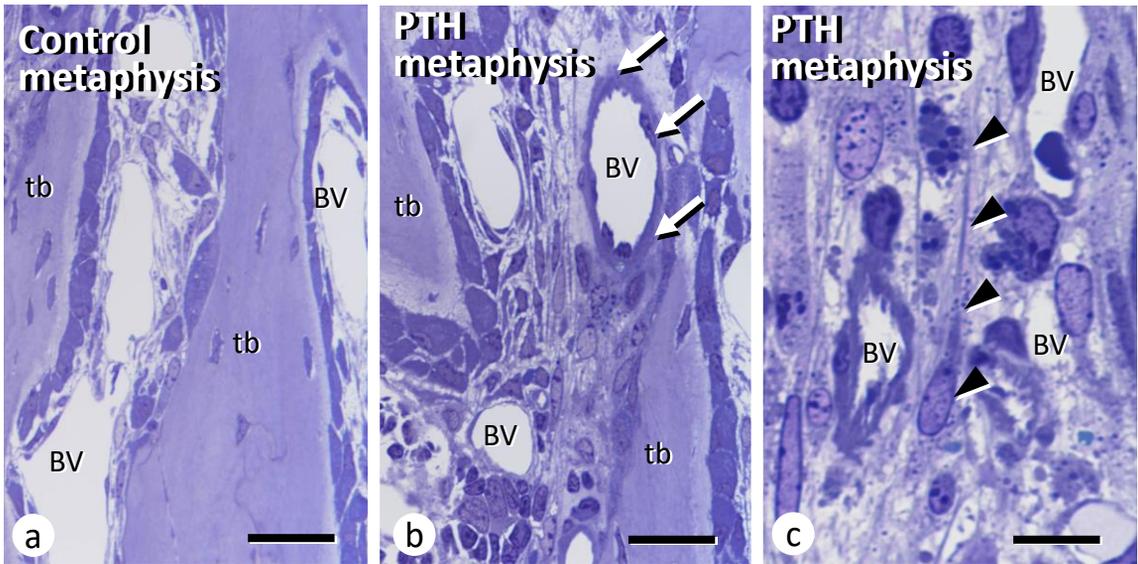
i

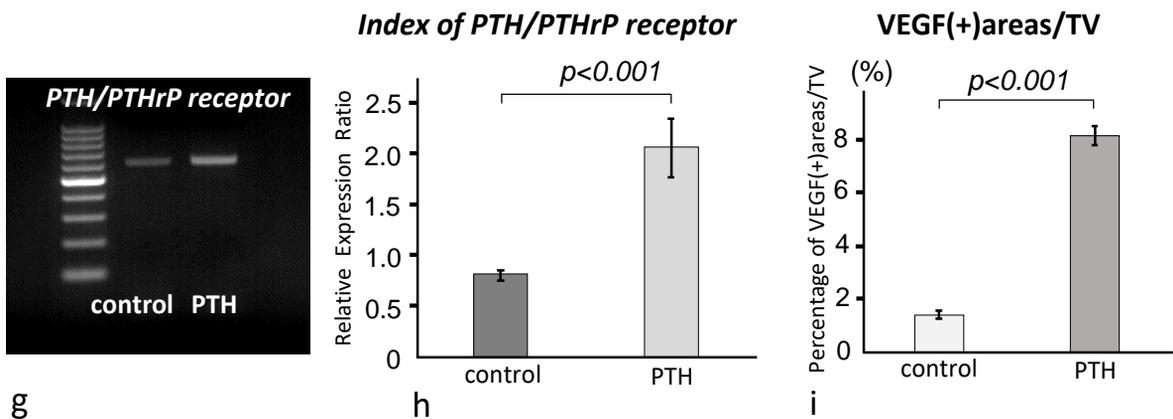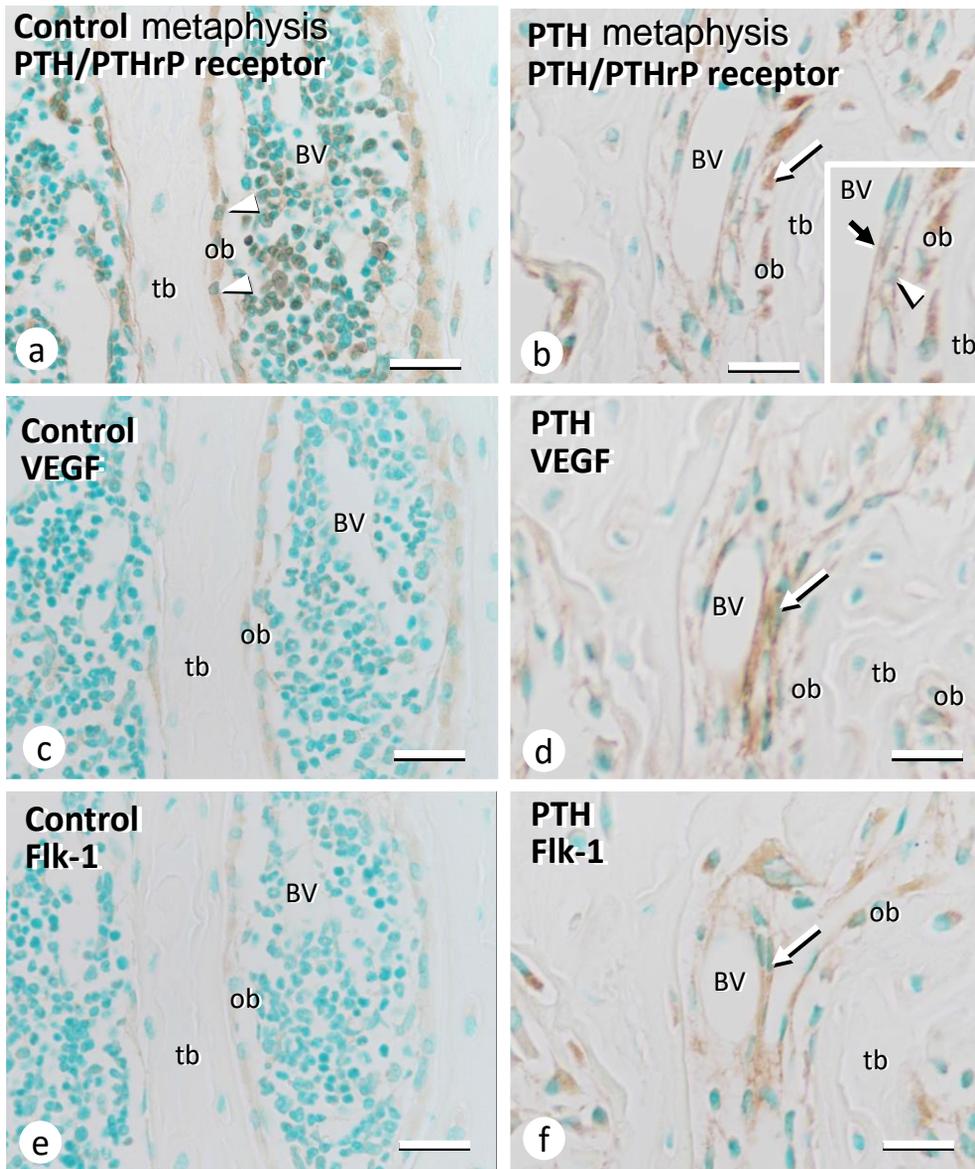Figure 7

Figure legends

Figure 1

Increased diameters of bone-specific blood vessels and immunodetection of αSMA-positive blood vessels after intermittent PTH administration

Panels **a-d** show the immunoreactivity of endomucin (brown color, **a** and **b**) and αSMA (brown color, **c** and **d**) in control (**a, c**) and PTH-treated (**b, d**) specimens, respectively. Note the enlarged endomucin-positive blood vessels (BV) in the PTH group (**b,** see the inset**)** compared with the control specimens (**a**, see the inset). αSMA-immunopositive blood vessels were markedly increased after PTH administration (**d**, see the arrows), while only a few αSMA-positive blood vessels were seen in control specimens (**c**). Panel **e** shows the statistical analysis of the maximum, minimum, and mean diameters of endomucin-reactive blood vessels in the ROI of control and PTH-treated specimens. There were significant differences in the maximum and mean diameter of endomucin-immunoreactive blood vessels between control and PTH-treated mice. Panel **f** verifies the area occupied by endomucin-reactive blood vessels in the control and PTH-treated groups. Notably, significantly increased indices were observed in the PTH-treated specimens.

tb: trabecular bone

Bar, **a-d**: 300 μm

Figure 2

Immunolocalization of endomucin-positive blood vessels and αSMA-immunoreactive cells after PTH administration.

Panels **a**, **b** show the double detection of endomucin (blue-purple color) and αSMA (brown color) via immunohistochemistry in control (**a**) and PTH-treated (**b**) specimens. The control specimens exhibited a small number of αSMA-positive cells (indicated with an arrow in **a**) surrounded by blood vessels (BV), while PTH-treated specimens exhibited many αSMA-positive cells (arrows, brown color in **b**) extended from endomucin-reactive blood vessels (indicated with an asterisk in **b**). Panels **c-e** are immunofluorescent microscopic images of the double detection of endomucin (red color) and αSMA (green color, white arrowheads) in control (**c**) and the PTH-treated specimens (**d**). When the PTH-treated metaphyses were

examined at a higher magnification, many αSMA-positive cells (green color, white arrows) were localized away from the blood vessels and featured a linear fibroblastic profile (**e**).

tb: trabecular bone

Bar, **a-d**: 50 μm, **e**: 10 μm

Figure 3

Distribution of ephrinB2-positive cells after PTH administration

Panels **a** and **b** show the double immunofluorescent detection of endomucin (red color) and ephrinB2 (green color) in control (**a**) and PTH-treated (**b**) specimens. Moreover, panels **c** and **d** represent the double immunofluorescent staining of αSMA (red color) and ephrinB2 (green color) in control (**c**) and PTH-treated (**d**) samples. In both the control and PTH groups, ephrinB2 reactivity can be seen in osteoblasts ("ob" in insets, **a**, **b**). In the PTH group, endomucin-positive blood vessels (red color, BV) were localized closer to ephrinB2-reactive osteoblasts (see inset in **b**). After PTH treatment, most αSMA-positive fibroblastic cells (red color) extending from the blood vessels intervened the cell layer of ephrinB2-reactive osteoblasts (green color) (see inset in **d**). In contrast, control specimens displayed only a few αSMA-reactive cells (red color, an arrow in the inset), which were restricted to the blood vessels (**c**).

tb: trabecular bone

Bar, **a-d**: 30 μm

Figure 4

Immunolocalization of EphB4 and statistical analyses of the numbers and gene expression of EphB4-, αSMA-, or endomucin-positive blood vessels

Panels **a-f** represent the immunofluorescent detection of endomucin (red color, **a**, **d**), EphB4 (green color, **b**, **e**), and merged images of endomucin and EphB4 (**c**, **f**) in control (**a-c**) and PTH-treated (**d-f**) specimens. EphB4 immunoreactivity (white arrows, **a**, **d**) can be seen mainly on endomucin-positive blood vessels (BV, white arrows in **b**, **e**) from both the control (**a**, **b**) and PTH (**d**, **e**) groups. The merged image shows the same localization of endomucin and EphB4 on blood vessels (white arrows, yellow color in **c, f**) in both the control (**c**) and PTH groups (**f**). Panel **g** is a statistical analysis of the number of EphB4-positive, αSMA-positive, and endomucin-positive blood vessels in the ROI of the control (dark gray bars) and PTH (light

gray bars) groups. Panel **h** presents the RT-PCR results of the *gapdh*, *endomucin*, *α-sma*, *ephrinb2*, and *Ephb4* genes between the control and PTH groups. Panels **i-l** represent the real-time PCR analyses of *endomucin*, *α-sma*, *ephrinb2,* and *Ephb4* gene expression after PTH administration.

tb: trabecular bone

Bar, **a-d**: 50 μm

Figure 5

Immunohistochemistry of TNALP, αSMA, and c-kit in the control and PTH-treated metaphyses

Panels **a**, **b** show the double detection of TNALP (blue-purple color) and αSMA (brown color) in control (**a**) and PTH-treated (**b**) specimens. In the control specimens, αSMA-positive cells were tightly associated with blood vessels (BV) (indicated with a white arrowhead in **a**), but not with TNALP-reactive osteoblasts (ob). After PTH administration, αSMA-positive cells (brown color, white arrows in **b**) extended from the blood vessels and appeared to intermingle with TNALP-reactive cells (blue-purple color), which are more broadly associated with the intertrabecular region (**b**). Panels **c** and **d** illustrate the immunodetection of c-kit (brown color) in control (**c**) and PTH-treated (**d**) specimens.   In the control metaphyses, a few fibroblastic cells (indicated with a white arrow) and bone marrow cells (white arrowheads) were positive for c-kit (**c**). After PTH administration, however, c-kit-reactive interstitial stromal cells (the arrow indicates the c-kit-positive cell area) were observed between the osteoblasts and blood vessels in the metaphyseal intertrabecular region (**d**). Panels **e** and **f** represent the statistical analyses of the TNALP(+)areas/TV and Ob.S/BS ratios, respectively.

tb: trabecular bone

Bar, **a-d**: 50 μm

Figure 6

Ultrastructure of interstitial stromal cells between blood vessels and osteoblasts in the intertrabecular region after PTH administration

Panels **a-c** are semi-thin sections of control (**a**) and PTH-treated (**b**, **c**) metaphyses stained with toluidine blue. Note that PTH-treated blood vessels (BV, white arrows in **b**) exhibited thicker

24

walls than those of the control blood vessels (**a**). At a higher magnification, spindle cell-types with long straight cytoplasmic processes (arrowheads in **c**) can be seen close to the blood vessels (BV, **c**). The TEM images show the elongated cytoplasmic processes of the interstitial cells (white arrows in **d**) and blood vessels surrounded with smooth muscle cells (white arrowheads in **d**). The long cytoplasmic processes (yellow-color) of the interstitial cells show cell-to-cell contact with other stromal cells and osteoblasts (**e**). A highly magnified image reveals the direct contact between the membranes of these cells (white arrowheads, **f**). Panel **g** is a highly-magnified image of the blood vessel shown in **d**. Vascular endothelial cells and vascular smooth muscle cells (red color) appeared to make partial contact with the bone surface. Bar, **a, b**: 30 μm, **c, d**: 10 μm, **e**: 3 μm, **f**: 2 μm, **g**: 5 μm

Figure 7

Immunolocalization of PTH/PTHrP receptor, VEGF, and Flk-1 in PTH-treated metaphyses
Panels **a-f** represent the immunolocalization of the PTH/PTHrP receptor (**a**, **b**), VEGF (**c**, **d**), and Flk-1 (**e**, **f**) on the serial sections of control (**a**, **c**, **e**) and PTH-treated (**b**, **d**, **f**) metaphyses. Notice that PTH/PTHrP receptor immunopositivity can be observed not only in osteoblasts on trabeculae (tb) but also in blood vessels (BV, indicated with a black arrow) and surrounding cells (indicated with a white arrowhead) in PTH-treated metaphysis (**b**), whereas the immunoreactivity was restricted to osteoblasts (arrowheads in **a**). The control metaphyses exhibited very faint VEGF-positivity (**c**) and Flk-1 immunoreactivity (**e**), whereas the PTH-treated metaphyses exhibited a relatively intense VEGF-positivity (indicated with a white arrow, **d**) and Flk-1 immunopositivity (indicated with a white arrow, **f**) mainly in blood vessels (BV) and nearby cells (white arrows), as well as osteoblasts (ob). Panels **g** and **h** represent the RT-PCR results and statistical analyses of PTH/PTHrP receptor expression estimated by real-time PCR. Panel **i** presents the statistical analyses of the VEGF(+)areas/TV indices.

Tb; trabecular bone

Bar, **a-f**: 20 μm